Materials Chemistry and Physics 263 (2021) 124390

Contents lists available at ScienceDirect

Materials Chemistry and Physics

journal homepage: www.elsevier.com/locate/matchemphys

Transient increase of T_c and J_c in superconducting/metallic heterostructures

A.M. Ionescu [a,b,*], M. Bihler [a], J. Simmendinger [a], C. Miksch [a], P. Fischer [a], G. Cristiani [c], K. S. Rabinovich [c], G. Schütz [a], J. Albrecht [d]

[a] Max Planck Institute for Intelligent Systems, Heisenbergstr. 3, D-70569, Stuttgart, Germany
[b] National Institute of Materials Physics, Atomistilor 405A, 077125, Magurele, Romania
[c] Max Planck Institute for Solid State Research, Heisenbergstr. 1, D-70569, Stuttgart, Germany
[d] Research Institute for Innovative Surfaces FINO, Aalen University, Beethovenstr. 1, D-73430, Aalen, Germany

HIGHLIGHTS

- Proximal metallic films can influence the properties of YBCO.
- A barrier layer between metal and YBCO was used.
- The deposition method of the metallic films plays a crucial role.
- Electron beam evaporation or ion beam sputtering were utilized for metal deposition.
- A transient increase of T_c and J_c was observed for samples prepared with evaporation.

ARTICLE INFO

Keywords:
Superconductor-metallic heterostructures
Critical temperature
Critical current density

ABSTRACT

The presence of a metallic layer can influence the properties of high-temperature superconductors underneath. We investigate the influence of metallic structures deposited in form of nanoparticles or continuous layers by electron beam evaporation or ion beam sputtering on the properties of $Y_1Ba_2Cu_3O_{7-x}$ (YBCO) thin films. To generally avoid diffusion of metal atoms an additional barrier layer is introduced. Detailed measurements of the magnetic moment of the superconductor as a function of temperature and magnetic field have been performed using SQUID magnetometry. It is found that the modification of the superconducting properties of coated YBCO strongly depends on the deposition method of the metal on top rather than the type of metal (Ni or Ag), its magnetic properties (ferromagnetic or paramagnetic) or its morphology (nanoparticles or thin film). The main result is a transient increase of the critical temperature T_c and critical current density J_c that was observed for samples prepared by electron beam evaporation.

1. Introduction

The discovery of superconductivity in $YBa_2Cu_3O_{7-x}$ (YBCO) with a transition temperature T_c of more than 90 K, well above the boiling point of liquid N_2, finally marked the beginning of the era of high-temperature superconductivity [1]. Among all high-temperature superconductors (HTS), YBCO is the most intensively studied due to its unique properties that are highly appealing for large-scale applications such as superconducting power cables, motors, magnetic energy-storage devices, fault current limiters and transformers [2–4].

The superconducting properties of YBCO are strongly correlated to the oxygen stoichiometry that can be adjusted over a wide range. Thus, the highest transition temperature $T_c = 93$ K is reached for the composition $YBa_2Cu_3O_{6.92}$, whereas for the oxygen content 7-x $<$ 6.4 the compound is not superconducting [5]. T_c is determined by both the hole concentration in the CuO_2 planes and the relative oxygen charge within the planes [6]. Oxygen diffusion can be enhanced by storage of YBCO films in vacuum or by direct irradiation with ultraviolet light (UV) [7].

In addition to high transition temperatures, application-ready superconductors also require in many cases a high flux pinning capability in large magnetic fields combined with a high irreversibility line. In the last few years several possibilities to suppress vortex motion have been

* Corresponding author. Max Planck Institute for Intelligent Systems, Heisenbergstr. 3, D-70569, Stuttgart, Germany.
E-mail address: ionescu@is.mpg.de (A.M. Ionescu).

https://doi.org/10.1016/j.matchemphys.2021.124390
Received 5 November 2020; Received in revised form 8 February 2021; Accepted 9 February 2021
Available online 11 February 2021

introduced leading to an increase of the superconducting critical current density, J_c [8]. A number of methods introducing natural and artificial pinning centers have been developed such as the creation of oxygen vacancies [9], microstructural variations [10,11], or the addition of secondary phases [12,13], magnetic nanoparticles or layers [14,15].

In particular, Ag is known to stabilize the oxygen content in cuprate superconductors [16]. The superconducting Ag composites are considered as potential candidates for technical applications due to their induced increase of the critical current density of YBCO films by up to 50% [17]. Furthermore, the normal state resistivity is lowered [18], a better chemical stability is reached and the mechanical strength increases [19].

Nickel atoms have been used for doping YBCO at the Cu site leading to a significant decrease of T_c. Although it has been found that for small doping concentrations the critical current density can be higher than for pure $YBa_2Cu_3O_{7-x}$ films a further increase of doping leads again to a drop [20].

Ni has a detrimental effect on YBCO for Rolling Assisted Biaxially Textured Substrate (RABiTS) tapes that require the deposition of oxide buffer layers [21].

Interesting results evolve from heterostructures formed of superconductors and metallic layers. If a ferromagnetic material is put in close contact with the superconductor a variety of coupling phenomena can take place such as proximity [22,23] and inverse proximity effects [24], spin-orbit [25] or dipolar coupling [26,27]. Thus, to avoid proximity effects [28] and to suppress diffusion of metal atoms a thin barrier layer is frequently introduced at the SC/FM interface [29]. This stops metal diffusion and limits possible superconductor-ferromagnetic (SC/FM) interaction to dipolar coupling [26,27].

In this work we investigate heterostructures of YBCO thin films grown by Pulsed Laser Deposition (PLD) and different metals. The metal structures in particular were deposited by two different techniques, namely electron beam evaporation and ion beam sputtering. Using magnetization and XRD measurements, we explore the impact of the type of metal (Ni or Ag), its magnetic properties (Ni as ferromagnetic and Ag as paramagnetic metal), its microstructure (nanoparticles and continuous film) and, finally, the deposition process on the superconducting properties of the YBCO film underneath. Contrary to most of other works where the metal was introduced in the YBCO matrix or deposited directly on top, we separate the materials by a thin barrier layer. Even if we can rule out proximity, inverse proximity and dipolar coupling effects, we still find systematic results that the deposited metal substantially influences the superconducting properties of YBCO films.

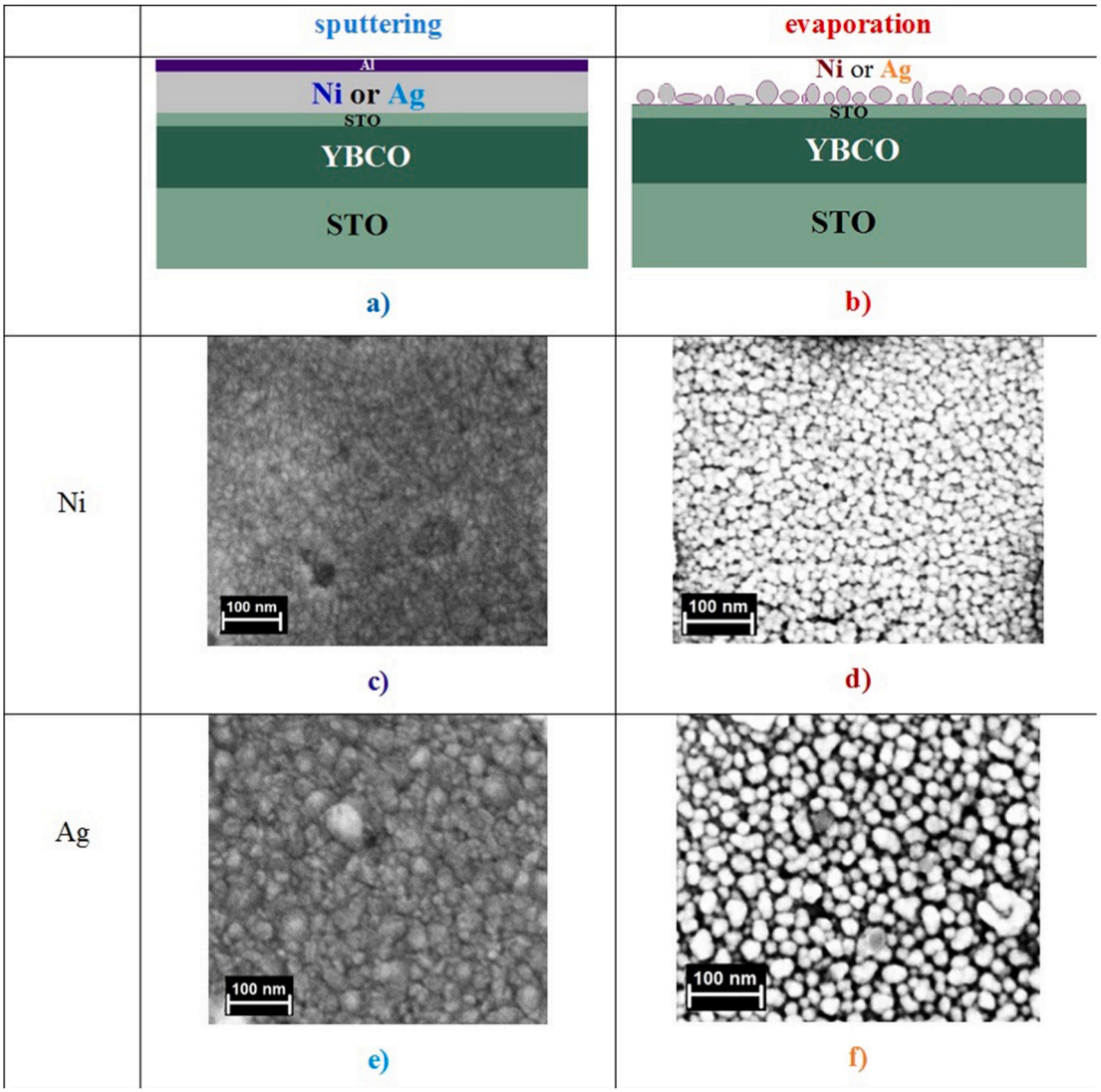

Fig. 1. Sketch of the sample stack for sputtered (a) and evaporated (b) metals; SEM images of the surface for (c) Ni layer, (d) Ni nanoparticles, (e) Ag layer and (f) Ag nanoparticles.

2. Results and discussion

Optimally doped YBCO thin films with a thickness of 200 nm were grown using pulsed-laser deposition (PLD) on single-crystalline $SrTiO_3$ (001) substrates with a lateral size of 5 × 5 mm^2. On top of the YBCO films a 5 nm STO barrier layer has been deposited by PLD to avoid proximity effects. The deposition of both layers was made at 830 °C in 0.3 mbar O_2 atmosphere, with a laser energy of 67 mJ, followed by annealing in 1 bar O_2.

Subsequently, Ni or Ag were deposited utilizing two different deposition techniques. We used first an electron beam evaporation technique, namely glancing angle deposition (GLAD) [30] to deposit Ni or Ag onto the superconductor. The glancing angle, here 83°, is chosen such that the material is deposited discontinuously on the substrate. Fast rotation of the substrate about its azimuthal axis is applied during the Ni or Ag deposition to obtain individual nanoparticles. Scanning electron micrographs are shown in Fig. 1 d) and f). The deposition was performed by electron-beam evaporation with a vacuum chamber pressure in the range of 10^{-6} mbar in a setup that has been described previously [30]. A thin layer of Ti was deposited both before the Ni or Ag growth to facilitate adhesion and after the Ni or Ag deposition to act as a protection layer. The randomly ordered Ni nanoparticles have diameters of 10–20 nm, in case of Ag we find 20–30 nm.

Second, for comparison, Ni and Ag layers of 50 nm thickness with a 2 nm Al capping layer were deposited using ion beam sputtering in UHV atmosphere at room temperature. With this method continuous thin films are obtained [31] and the morphology is visualized in Fig 1 c) and e).

We will further refer to the samples prepared with electron beam evaporation as *evaporation* and to the ion beam sputtered samples with the abbreviation *sputtering*. The sketch of the sample stack can be seen in Fig. 1 for sputtering (a) or evaporation (b), with the corresponding SEM images for (c) Ni layer, (d) Ni nanoparticles, (e) Ag layer and (f) Ag nanoparticles.

All samples have been characterized by SQUID magnetometry using a Quantum Design MPMS3. For our purpose, magnetization measurements were preferred to transport ones to exclude the contribution of the metal. The external magnetic field $\mu_0 H$ was always applied perpendicular to the plane of the sample. To measure T_c, the samples were zero-field cooled (ZFC) to T = 5 K, a small field of 1 mT was applied and the temperature was increased to 100 K while measuring the magnetic moment $m(T)$. At the superconducting transition temperature the diamagnetic signal vanishes. To better reveal the influence of different metallic layers on the superconducting properties of YBCO corresponding hysteresis loops have been measured at 25 K and 85 K and the value at remanence has been extracted. To determine the critical current density J_c the Bean relation has been applied [32] modified for a plate-like geometry [33]:

$$J_c(\mathrm{A/cm^2}) = 60|m(emu)|/\mathrm{V(cm^3)} \cdot \mathrm{l(cm)};$$

where V refers to the sample volume and l is the lateral size of the square.

The microstructure of the heterostructures has been analyzed by high-resolution X-ray diffraction (XRD) using Cu Kα radiation in the range 2θ = 10°–60°.

Fig. 2 presents examples of the magnetization measurements conducted for all samples. In panel a) typical $m(T)$ curves in an applied field of 1 mT under ZFC conditions are shown. Black (solid square, solid line) refers to results obtained with a pristine YBCO sample ("before"), after the deposition of Ni nanoparticles using electron beam evaporation the films are immediately remeasured (brown open square, dashed line, Ni deposition, time 0), finally red (triangle, dotted line) depicts the behavior after some time ("after", expressed in weeks).

Two main results can be extracted from Fig. 2 a): First, the onset of the transition is significantly shifted to higher temperatures in case of Ni (brown) and, second, the transition is much broader in case of the aged curve (red). Note, a sharp transition refers to a homogenous sample. To better emphasize changes in T_c we show the time development of T_c in the inset using corresponding colors. A significant increase of T_c of ~3 K (from solid, black square to open brown) is observed after the deposition of Ni nanoparticles followed by a drop until the initial value is reached again in the measurement after 22 weeks (triangles, red). To correlate this with the magnetic moment we measured the corresponding hysteresis curves at elevated temperatures, T = 85 K. Here, the basic behaviour is the same: a significant increase of m after Ni deposition (of 54% at $\mu_0 H$ = 0 mT) is followed by a strong decrease after 22 weeks (81% at $\mu_0 H$ = 0 mT). Correlating the shape of the dotted red curve in Fig. 2 a) with the serious decrease of m at 85 K in panel b), we assume that the observed behaviour originates either due to change of the oxygen content in the crystalline lattice of YBCO or by the introduction of additional pinning sites that change over time.

To check if the surprising increase of the superconducting properties after the deposition of Ni nanoparticles using evaporation is due to the specific deposition technique and not due to the ferromagnetic behavior of Ni we replaced Ni by Ag and also analyzed YBCO with Ag nanoparticles prepared with evaporation. In addition, YBCO/Ni and YBCO/Ag closed layers were deposited using classical ion beam sputtering.

Fig. 3 depicts the time evolution of T_c and J_c. The latter is extracted from the hysteresis curves at 85 K in zero field (decreased from high fields). Panels c) and d) are a different representation of a) and b) where T_c and J_c are normalized to their initial values before deposition. Red, full symbols represent results of evaporated samples and blue, open symbols, refer to sputtered samples. Squares denote YBCO/Ni and circles refer to YBCO/Ag. The dashed lines serve as guide to the eye.

A significant increase of T_c of ~3 K appears immediately after

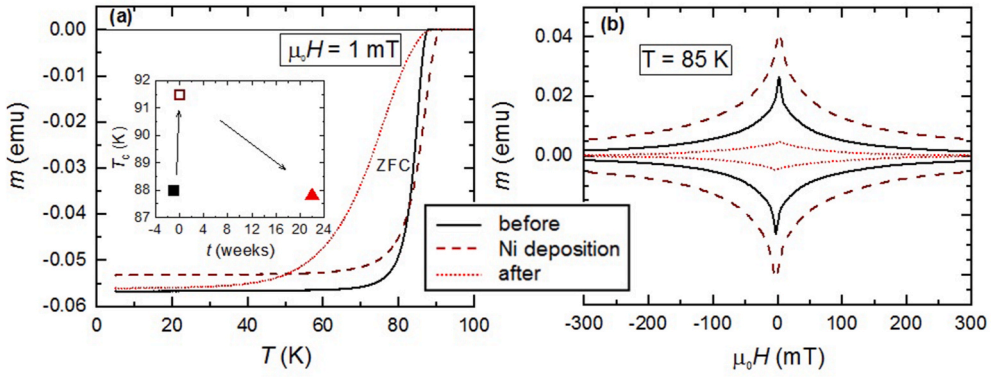

Fig. 2. a) m(T) in an applied filed of $\mu_0 H$ = 1 mT under ZFC conditions. T_c is extracted for a YBCO reference sample (before), immediately after deposition of Ni nanoparticles with evaporation (Ni deposition) and re-measured after 22 weeks (after). b) The corresponding hysteresis loops at 85 K show a substantial increase of the magnetization immediately after Ni deposition is observed.

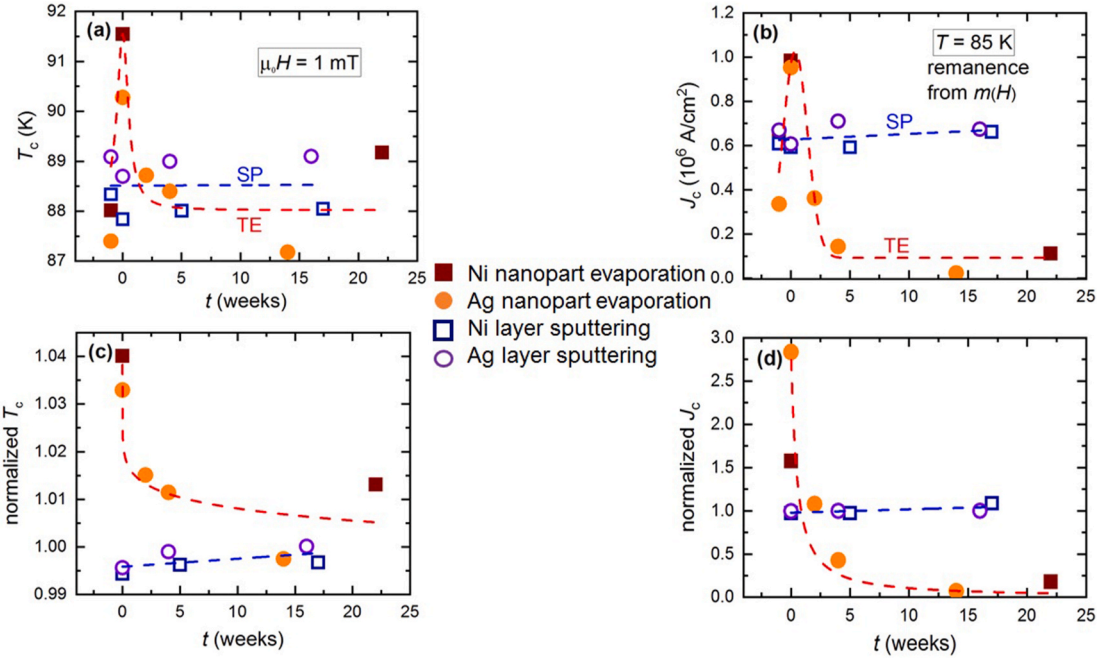

Fig. 3. *a) Time evolution of T_c, the first points correspond to the initial measurements of pristine YBCO samples, 0 marks the measurement after deposition of Ni or Ag and the other values refer to measurements after several weeks. b) J_c at 85 K extracted from the hysteresis curves in remanent state. c) and d) depict a different representation of a) and b) where the data are normalized to the initial values before deposition, M is Ag or Ni. Dashed lines are guide to the eyes. Blue refers to sputtered metals, red to evaporated ones.* (For interpretation of the references to color in this figure legend, the reader is referred to the Web version of this article.)

deposition of Ni or Ag on top of YBCO for samples deposited using electron beam evaporation under glancing angles. After some time this increase decays and finally reaches the initial value. A similar behaviour is observed for the critical current density $J_c(t)$ as well, however here, the final decay is more prominent. It is found that the values of J_c almost vanish at $T = 85$ K.

Identical metals were used for deposition by ion beam sputtering. In this case, no significant change in T_c or J_c is observed. This leads to the conclusion that the deposition technique of the metal plays an important role for the consequences on the superconducting properties of YBCO.

We extracted the critical current density from the hysteresis curves at $T = 25$ K and $T = 85$ K as done before and represented it as a function of time. Full symbols give the samples prepared with evaporation and open symbols refer to the sputtered films. In addition, data of two more samples are included, namely continuous Ni films prepared by evaporation. One film has been deposited at room temperature and another film while cooling the substrate by LN2.

As can be observed in Fig. 4 a), J_c shows a considerable decrease for the evaporated samples at $T = 25$ K while no change is detected for the sputtered metals. At $T = 85$ K, a significant increase (up to a factor of 3 for the sample with Ag nanoparticles) was noticed, followed also by a decrease after some time.

Since all evaporated samples exhibit the same phenomenology we can rule out the influence of microstructure (nanoparticles or layers), magnetism (ferromagnetic or paramagnetic) or deposition temperature (room temperature or cooled). In case of the sputtered films no significant degradation after deposition or in time is found.

In a next step we performed XRD in a θ - 2θ geometry to evaluate if the observed effects are related to structural variations in the superconductor. In particular, it is desirable to obtain information about the oxygen distribution inside the film. At the same time information about additional stress due to the deposition of a metallic layer on top of YBCO might be obtained.

The following three samples have been thoroughly analyzed: a pristine YBCO film (green, solid line, solid circle), a YBCO/Ni nanoparticle heterostructure (Ni deposited with evaporation (brown, dashed

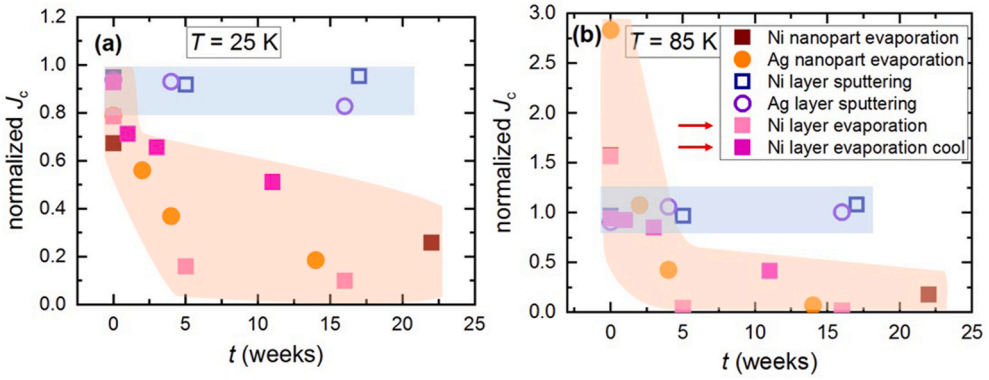

Fig. 4. *Time evolution of the normalized J_c at 25 K and 85 K extracted from hysteresis loops. Light and dark pink symbols refer to continuous thin films prepared by regular evaporation, one at room temperature and one cooled with LN2, to investigate the effect of microstructure of the metallic film and the temperature during deposition.* (For interpretation of the references to color in this figure legend, the reader is referred to the Web version of this article.)

line, solid square)) and a YBCO/continuous Ni layer deposited using sputtering (blue, dash dotted line, open square). Both YBCO films with capping layers were measured after an ageing time of several months.

All spectra depicted in Fig. 5 exhibit the typical features of a c-axis oriented epitaxial YBCO film. As expected, YBCO grew crystalline along the (00l) direction on the STO substrate. Shape and intensity of the peaks for the pristine YBCO and the sputtered Ni layer are very similar. The only difference is a slight shift of the peaks towards higher angles in case of the sputtered Ni. The shape of the peaks for the YBCO and the sputtered Ni layer indicates good homogeneity of the crystalline structure. There are no pronounced Ni peaks in the spectrum suggesting that Ni has an amorphous structure. The shift of the YBCO peaks to higher angles in case of the sputtered Ni layer refers to a slightly reduced c-axis which, according to Ref. [34], might correspond to a marginally higher oxygen content. However, this change would be too small to result in a detectable shift of T_c.

In contrast, we observe a significant widening of all (00n) peaks in case of the YBCO film decorated with Ni nanoparticles from glancing angle evaporation. In particular, the (004) peak shows an increase of the FWHM by a factor of 5. This directly refers to structural inhomogeneities in the film, namely local variations of the lattice parameters of YBCO. An explanation could be given by an inhomogeneous oxygen distribution in the YBCO film, namely a gradual change of the oxygen content over the whole thickness. This is supported by the shape of $m(T)$ curve in Fig. 2 as well which clearly shows a significantly enhanced transition width indicating inhomogeneous properties.

To find possible reasons for the increase of T_c of up to 3 K for particular YBCO heterostructures we performed different experimental steps: a large increase of T_c has been found in YBCO/STO bilayers decorated with electron beam evaporated Ni nanoparticles. An analogous sample using Ag instead of Ni prepared by evapoation has been analyzed and showed equivalent results. This rules out that the ferromagnetism in Ni plays a role for the effect.

Replacing Ni nanoparticles by a continuous layer of Ni, also deposited by electron beam evaporation, led to a significant increase of the transition temperature as well. The morphology of the deposited metal is not relevant for the superconducting transition temperature.

A possible effect of heating during deposition is addressed by equivalently prepared films with additional cooling by LN2 during deposition. Since no significant change of the results has been found heat is ruled out as driving force for the observed effects.

Having these reasons eliminated and further analyzing the results we are able to make several statements: The increase of T_c leads to an increase of J_c at high temperatures whereas at low temperatures of $T = 25$ K only decreasing values of J_c are found. This shows that there is no general increase of pinning, at low temperatures a decrease of intrinsic pinning is responsible for a lower J_c.

Since the STO barrier layer prevents metal diffusion into the YBCO layer the structural changes observed by XRD have to have another reason. It was observed that ageing of several weeks under ambient conditions led to a drastic degradation of the superconducting properties. The shape of the $m(T)$ curves changing over time suggests that there is a change in the oxygen content in YBCO film. Oxygen transfer from YBCO to the metal is only possible if the STO barrier allows significant oxygen diffusion at room temperature.

Since it has been observed that oxygen diffusion can be supported as well by storage of the YBCO films in vacuum or by direct irradiation with ultraviolet light (UV) [7] we kept an YBCO film in the evaporation chamber during one of the other depositions. It was found that neither UV nor high vacuum treatments contribute significantly to the observed behavior of YBCO.

Results basically change when the metallic layer has been deposited by ion beam sputtering. Here, the superconducting properties of YBCO remained unchanged and the shift of T_c and J_c was absent. The important difference between both deposition techniques is the kinetic energy of the particles during deposition on top of the STO surface. For the sputtering process this energy is large enough to create structural damage by collisions at the surface of the STO. We consider oxygen diffusion as major mechanism leading to a transient increase of T_c and J_c of high-quality superconducting YBCO films when depositing an STO and a metallic layer. This means that oxygen motion occurs from the YBCO via a thin STO layer to the deposited metal. Surface damage induced by high energy particles in the sputtering process is assumed to inhibit the oxygen diffusion.

3. Conclusions

In summary, we found a large influence of various metallic coatings on critical current density and critical temperature of high-temperature superconducting YBCO thin films even when separated by a 5 nm barrier layer of STO. Two techniques have been used for the deposition of metals (Ni and Ag), namely electron beam evaporation with Glancing Angle Deposition to form nanoparticles and ion beam sputtering. From SQUID measurements it is found that the modification of the superconducting properties in these heterostructures might be explained by the conditions specific to the deposition technique and not on the type of metal, its magnetic properties (ferromagnetic or paramagnetic) or its morphology (nanoparticles or thin films). We observed a transient increase of T_c and J_c for films prepared with electron beam evaporation, followed by a depression of the superconducting properties after some ageing time. For ion beam sputtered samples no significant change has been noticed. Evaporation might support oxygen diffusion through the barrier STO layer leading to changes in J_c and T_c over time. A next step will be the preparation of heterostructures that conserve the increase of

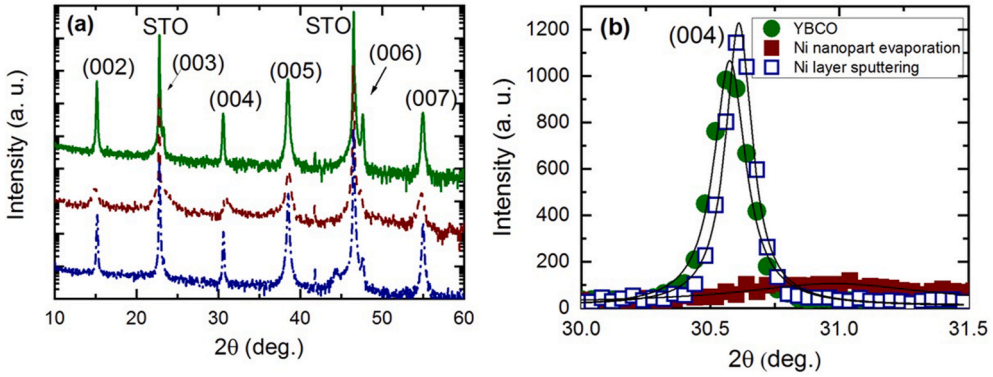

Fig. 5. a) XRD pattern for a YBCO film (green), YBCO/Ni nanoparticles prepared by glancing angle evaporation (brown) after 22 weeks and YBCO/Ni layer deposited using sputtering (blue) after 17 weeks b) Magnification of the (004) peak. (For interpretation of the references to color in this figure legend, the reader is referred to the Web version of this article.)

a high T_c of $T_c = 92$ K and thus high values of J_c at temperatures of 77 K and above.

CRediT authorship contribution statement

A.M. Ionescu: Formal analysis, Data curation, performed the magnetic measurements, All authors contributed extensively to the work presented in this paper, discussed the results and implications and commented on the manuscript at all stages. **M. Bihler:** Formal analysis, Data curation, All authors contributed extensively to the work presented in this paper, discussed the results and implications and commented on the manuscript at all stages. **J. Simmendinger:** prepared the manuscript, All authors contributed extensively to the work presented in this paper, discussed the results and implications and commented on the manuscript at all stages. **C. Miksch:** prepared the metallic layers by electron beam sputtering, All authors contributed extensively to the work presented in this paper, discussed the results and implications and commented on the manuscript at all stages. **P. Fischer:** Conceptualization, All authors contributed extensively to the work presented in this paper, discussed the results and implications and commented on the manuscript at all stages. **G. Cristiani:** prepared the YBCO and STO layers by PLD, All authors contributed extensively to the work presented in this paper, discussed the results and implications and commented on the manuscript at all stages. **K.S. Rabinovich:** made XRD measurements, All authors contributed extensively to the work presented in this paper, discussed the results and implications and commented on the manuscript at all stages. **G. Schütz:** Conceptualization, Data curation, All authors contributed extensively to the work presented in this paper, discussed the results and implications and commented on the manuscript at all stages. **J. Albrecht:** Conceptualization, Data curation, All authors contributed extensively to the work presented in this paper, discussed the results and implications and commented on the manuscript at all stages.

Declaration of competing interest

The authors declare that they have no known competing financial interests or personal relationships that could have appeared to influence the work reported in this paper.

Acknowledgements

The authors are grateful to B. Ludescher for his contribution to the sample fabrication and to Dr. H.N. Barad for the fruitful discussions (MPI Stuttgart).

This research did not receive any specific grant from funding agencies in the public, commercial, or not-for-profit sectors.

References

[1] M.K. Wu, J.R. Ashburn, C.J. Torng, P.H. Hor, R.L. Meng, L. Gao, Z.J. Huang, Y. Q. Wang, C.W. Chu, Superconductivity at 93 K in a new mixed-phase Yb-Ba-Cu-O compound system at ambient pressure, Phys. Rev. Lett. 58 (1987) 908–910, https://doi.org/10.1103/PhysRevLett.58.908.

[2] S.R. Foltyn, L. Civale, J.L. Macmanus-Driscoll, Q.X. Jia, B. Maiorov, H. Wang, M. Maley, Materials science challenges for high-temperature superconducting wire, Nat. Mater. 6 (2007) 631–642, https://doi.org/10.1142/9789814317665_0045.

[3] D. Larbalestier, A. Gurevich, D.M. Feldmann, A. Polyanskii, High-Tc superconducting materials for electric power applications, Nature 414 (2001) 368–377, https://doi.org/10.1038/35104654.

[4] P. Seidel, Applied Superconductivity: Handbook on Devices and Applications, Wiley, 2015.

[5] K. Conder, Oxygen diffusion in the superconductors of the YBaCuO family: isotope exchange measurements and models. https://doi.org/10.1016/S0927-796X(00)00030-9, 2001.

[6] M. Karppinen, H. Yamauchi, Hole-doping routes for understanding the relationship between atomic arrangements and superconductivity properties in multi-layered copper oxides, Int. J. Inorg. Mater. 2 (2000) 589–599, https://doi.org/10.1016/S1466-6049(00)00085-4.

[7] R. Mogilevsky, R. Levi-Setti, B. Pashmakov, L. Liu, K. Zhang, H.M. Jaeger, D. B. Buchholz, R.P.H. Chang, B.W. Veal, Direct measurements ofroom-temperature oxygen diffusion in YBa2Cu3OX, Phys. Rev. B 49 (1994) 6420, https://doi.org/10.1103/PhysRevB.49.6420.

[8] A.K. Jha, K. Matsumoto, Superconductive REBCO thin films and their nanocomposites: the role of rare-earth oxides in promoting sustainable energy, Front. Physiol. 7 (2019) 1–21, https://doi.org/10.3389/fphy.2019.00082.

[9] H. Theuss, H. Kronmüller, The influence of a point defect structure on the magnetic properties of YBa2Cu3O7-δ polycrystals, Phys. C. 177 (1991) 253–261, https://doi.org/10.1016/0921-4534(91)90323-Q.

[10] H. Yan, M.M. Abdelhadi, J.A. Jung, B.A. Willemsen, K.E. Kihlstrom, Exponential dependence of the vortex pinning potential on current density in high- Tc superconductors, Phys. Rev. B 72 (2005), https://doi.org/10.1103/PhysRevB.72.064522, 064522.

[11] C. Jooss, R. Warthmann, H. Kronmüller, T. Haage, H.U. Habermeier, J. Zegenhagen, Vortex pinning due to strong quasiparticle scattering at antiphase boundaries in YBa2Cu3O7−δ, Phys. Rev. Lett. 82 (1999) 632–635, https://doi.org/10.1103/PhysRevLett.82.632.

[12] L. Opherden, M. Sieger, P. Pahlke, R. Hühne, L. Schultz, A. Meled, G. Van Tendeloo, R. Nast, B. Holzapfel, B. Marco, J.L. Macmanus, J. Hänisch, Large pinning forces and matching effects in YBa2Cu3O7- δ thin films with Ba2Y(Nb/Ta)O6 nano- precipitates, Sci. Rep. 6 (2016), https://doi.org/10.1038/srep21188, 21188.

[13] A. Crisan, V.S. Dang, P. Mikheenko, A.M. Ionescu, I. Ivan, L. Miu, Synergetic pinning centres in BaZrO3-doped YBa2Cu3O7-x films induced by SrTiO3 nano-layers, Supercond. Sci. Technol. 30 (2017), https://doi.org/10.1088/1361-6668/aa5edf, 045012.

[14] V. Rouco, R. Córdoba, J.M. De Teresa, L.A. Rodríguez, C. Navau, N. Del-Valle, G. Via, A. Sánchez, C. Monton, F. Kronast, X. Obradors, T. Puig, A. Palau, Competition between Superconductor – ferromagnetic stray magnetic fields in YBa2Cu3O7−x films pierced with Co nano-rods, Sci. Rep. 7 (2017) 5663, https://doi.org/10.1038/s41598-017-05909-6.

[15] C. Stahl, P. Walker, S. Treiber, G. Christiani, G. Schütz, J. Albrecht, Using magnetic coupling in bilayers of superconducting YBCO and soft-magnetic CoFeB to map supercurrent flow, Epl 106 (2014), https://doi.org/10.1209/0295-5075/106/27002, 27002.

[16] D. Behera, S.K. Dash, N.C. Mishra, Effect of Ag in controlling self-field induced flux creep in Y1−xCaxBa2Cu3O7−y systems, Phys. Lett. 300 (2002) 529–537, https://doi.org/10.1016/S0375-9601(02)00470-X.

[17] M. Kienzle, J. Albrecht, R. Warthmann, H. Kronmüller, S. Leonhardt, C. Jooss, Enhanced critical currents by silver sheeting of (formula presented) thin films, Phys. Rev. B - Condens. Matter Mater. Phys. 66 (2002) 1–7, https://doi.org/10.1103/PhysRevB.66.054525.

[18] N.C. Mishra D. Behera, 1 K. Patnaik, DC electrical resistivity study of granularity in YBa2Cu3O7/Ag composites, J. Supercond. 11 (1998) 641–648, https://doi.org/10.1557/proc-99-961.

[19] R.V.R. Pinto, P.R. Apte, M.S.R. Rao, Ramesh Chandra, C.P. D'Souza, S.P. Pai, L. C. Gupta, Superconductivity and transport behavior of laser ablated Au-added YBa2Cu3O7-d thin film, Appl. Phys. Lett. 68 (68) (1996) 1006–1008, https://doi.org/10.7868/s0367676514080183.

[20] H. Afifi, I. Hager, S. Naqib, Structural, Electrical, Magnetic, and Flux Pinning Properties of YBCO/Ni Superconducting Composites: Analyses and Possible Explanations, 2018, pp. 1–19.

[21] D. Selbmann, J. Eickemeyer, H. Wendrock, NiO layers on Ni RABiTS for epitaxial buffer deposition by LS MOCVD, J. Phys. IVFrance. 11 (2001) 239–245, https://doi.org/10.1051/jp4:20011139.

[22] D.K. Satapathy, M.A. Uribe-Laverde, I. Marozau, V.K. Malik, S. Das, T. Wagner, C. Marcelot, J. Stahn, S. Brück, A. Rühm, S. Macke, T. Tietze, E. Goering, A. Frañó, J.-H. Kim, M. Wu, E. Benckiser, B. Keimer, A. Devishvili, B.P. Toperverg, M. Merz, P. Nagel, S. Schuppler, C. Bernhard, Magnetic proximity effect in YBa2Cu3O7/La2/3Ca1/3MnO3 and YBa2Cu3O7/LaMnO3+δ superlattices, Phys. Rev. Lett. 108 (2012), https://doi.org/10.1103/physrevlett.108.197201, 197201.

[23] A. Frano, S. Blanco-Canosa, E. Schierle, Y. Lu, M. Wu, M. Bluschke, M. Minola, G. Christiani, H.U. Habermeier, G. Logvenov, Y. Wang, P.A. Van Aken, E. Benckiser, E. Weschke, M. Le Tacon, B. Keimer, Long-range charge-density-wave proximity effect at cuprate/manganate interfaces, Nat. Mater. 15 (2016) 831–834, https://doi.org/10.1038/nmat4682.

[24] Y. Kalcheim, O. Millo, A. Di Bernardo, A. Pal, J.W.A. Robinson, Inverse proximity effect at superconductor-ferromagnet interfaces: evidence for induced triplet pairing in the superconductor, Phys. Rev. B - Condens. Matter Mater. Phys. 92 (2015), https://doi.org/10.1103/PhysRevB.92.060501, 060504(R).

[25] N. Banerjee, J.A. Ouassou, Y. Zhu, N.A. Stelmashenko, J. Linder, M.G. Blamire, Controlling the superconducting transition by spin-orbit coupling, Phys. Rev. B 97 (2018), https://doi.org/10.1103/PhysRevB.97.184521, 184521.

[26] J. Brisbois, M. Motta, J.I. Avila, G. Shaw, T. Devillers, N.M. Dempsey, S.K. P. Veerapandian, P. Colson, B. Vanderheyden, P. Vanderbemden, W.A. Ortiz, N. D. Nguyen, R.B.G. Kramer, A. V Silhanek, Imprinting superconducting vortex footsteps in a magnetic layer, Sci. Rep. 6 (2016), https://doi.org/10.1038/srep27159, 27159.

[27] A.Y. Aladyshkin, A.V. Silhanek, W. Gillijns, V.V. Moshchalkov, Nucleation of superconductivity and vortex matter in superconductor- ferromagnet hybrids, Supercond. Sci. Technol. 22 (2009), https://doi.org/10.1088/0953-2048/22/5/053001, 053001.

[28] T.Y. Chien, L.F. Kourkoutis, J. Chakhalian, B. Gray, M. Kareev, N.P. Guisinger, D. A. Muller, J.W. Freeland, Superconducting oxides, Nat. Commun. 4 (2013) 1–7, https://doi.org/10.1038/ncomms3336.

[29] J. Albrecht, S. Soltan, H.U. Habermeier, Magnetic pinning of flux lines in heterostructures of cuprates and manganites, Phys. Rev. B 72 (2005), https://doi.org/10.1103/PhysRevB.72.092502, 092502.
[30] A.G. Mark, J.G. Gibbs, T.C. Lee, P. Fischer, Hybrid nanocolloids with programmed three-dimensional shape and material composition, Nat. Mater. 12 (2013) 802–807, https://doi.org/10.1038/nmat3685.
[31] P. Farber, H. Kronmüller, Thickness dependence of magnetoelastic properties and of crystallization behavior in Fe–Tb–Dy/Fe and Fe–Tb–Dy/nanocrystalline Fe–Si–B–Nb–Cu multilayers, J. Appl. Phys. 88 (2000) 2781–2786, https://doi.org/10.1063/1.1287775.
[32] C.P. Bean, Magnetization of hard superconductors, Phys. Rev. Lett. 8 (1962) 250–253, https://doi.org/10.1103/PhysRevLett.8.250.
[33] E.M. Gyorgy, R.B. Van Dover, K.A. Jackson, L.F. Schneemeyer, J.V. Waszczak, Anisotropic critical currents in Ba2YCu3O7analyzed using an extended Bean model, Appl. Phys. Lett. 55 (1989) 283–285, https://doi.org/10.1063/1.102387.
[34] P. Benzi, E. Bottizzo, N. Rizzi, Oxygen determination from cell dimensions in YBCO superconductors, J. Cryst. Growth 269 (2004) 625–629, https://doi.org/10.1016/j.jcrysgro.2004.05.082.